Emissions pathways, climate change, and impacts on California

Katharine Hayhoe[a,b], Daniel Cayan[c], Christopher B. Field[d], Peter C. Frumhoff[e], Edwin P. Maurer[f], Norman L. Miller[g], Susanne C. Moser[h], Stephen H. Schneider[i], Kimberly Nicholas Cahill[d], Elsa E. Cleland[d], Larry Dale[g], Ray Drapek[j], R. Michael Hanemann[k], Laurence S. Kalkstein[l], James Lenihan[j], Claire K. Lunch[d], Ronald P. Neilson[j], Scott C. Sheridan[m], and Julia H. Verville[e]

[a]ATMOS Research and Consulting, 809 West Colfax Avenue, South Bend, IN 46601; [c]Climate Research Division, The Scripps Institution of Oceanography, and Water Resources Division, U.S. Geological Survey, 9500 Gilman Drive, La Jolla, CA 92093-0224; [d]Department of Global Ecology, Carnegie Institution of Washington, 260 Panama Street, Stanford, CA 94305; [e]Union of Concerned Scientists, Two Brattle Square, Cambridge, MA 02238; [f]Civil Engineering Department, Santa Clara University, Santa Clara, CA 95053; [g]Atmosphere and Ocean Sciences Group, Earth Sciences Division, Lawrence Berkeley National Laboratory, 1 Cyclotron Road, Berkeley, CA 94720; [h]Environmental and Societal Impacts Group, National Center for Atmospheric Research, P.O. Box 3000, Boulder, CO 80307; [i]Department of Biological Sciences and Institute for International Studies, Stanford University, Stanford, CA 94305; [j]Corvallis Forestry Sciences Laboratory, U.S. Department of Agriculture Forest Service, 3200 SW Jefferson Way, Corvallis, OR 97331; [k]Department of Agricultural and Resource Economics, University of California, Berkeley, CA 94720; [l]Center for Climatic Research, Department of Geography, University of Delaware, Newark, DE 19716; and [m]Department of Geography, Kent State University, Kent, OH 44242

Contributed by Christopher B. Field, June 23, 2004

The magnitude of future climate change depends substantially on the greenhouse gas emission pathways we choose. Here we explore the implications of the highest and lowest Intergovernmental Panel on Climate Change emissions pathways for climate change and associated impacts in California. Based on climate projections from two state-of-the-art climate models with low and medium sensitivity (Parallel Climate Model and Hadley Centre Climate Model, version 3, respectively), we find that annual temperature increases nearly double from the lower B1 to the higher A1fi emissions scenario before 2100. Three of four simulations also show greater increases in summer temperatures as compared with winter. Extreme heat and the associated impacts on a range of temperature-sensitive sectors are substantially greater under the higher emissions scenario, with some interscenario differences apparent before midcentury. By the end of the century under the B1 scenario, heatwaves and extreme heat in Los Angeles quadruple in frequency while heat-related mortality increases two to three times; alpine/subalpine forests are reduced by 50–75%; and Sierra snowpack is reduced 30–70%. Under A1fi, heatwaves in Los Angeles are six to eight times more frequent, with heat-related excess mortality increasing five to seven times; alpine/subalpine forests are reduced by 75–90%; and snowpack declines 73–90%, with cascading impacts on runoff and streamflow that, combined with projected modest declines in winter precipitation, could fundamentally disrupt California's water rights system. Although interscenario differences in climate impacts and costs of adaptation emerge mainly in the second half of the century, they are strongly dependent on emissions from preceding decades.

California, with its diverse range of climate zones, limited water supply, and economic dependence on climate-sensitive industries such as agriculture, provides a challenging test case to evaluate impacts of regional-scale climate change under alternative emissions pathways. As characterized by the Intergovernmental Panel on Climate Change, demographic, socioeconomic, and technological assumptions underlying long-term emissions scenarios vary widely (1). Previous studies have not systematically examined the difference between projected regional-scale changes in climate and associated impacts across scenarios. Nevertheless, such information is essential to evaluate the potential for and costs of adaptation associated with alternative emissions futures and to inform mitigation policies (2).

Here, we examine a range of potential climate futures that represent uncertainties in both the physical sensitivity of current climate models and divergent greenhouse gas emissions pathways. Two global climate models, the low-sensitivity National Center for Atmospheric Research/Department of Energy Parallel Climate Model (PCM) (3) and the medium-sensitivity U.K. Met Office Hadley Centre Climate Model, version 3 (HadCM3), model (4, 5) are used to calculate climate change resulting from the SRES (Special Report on Emission Scenarios) B1 (lower) and A1fi (higher) emissions scenarios (1). These scenarios bracket a large part of the range of Intergovernmental Panel on Climate Change nonintervention emissions futures with atmospheric concentrations of CO_2 reaching ≈550 ppm (B1) and ≈970 ppm (A1fi) by 2100 (see *Emissions Scenarios* in *Supporting Text*, which is published as supporting information on the PNAS web site). Although the SRES scenarios do not explicitly assume any specific climate mitigation policies, they do serve as useful proxies for assessing the outcome of emissions pathways that could result from different emissions reduction policies. The scenarios at the lower end of the SRES family are comparable to emissions pathways that could be achieved by relatively aggressive emissions reduction policies, whereas those at the higher end are comparable to emissions pathways that would be more likely to occur in the absence of such policies.

Climate Projections

Downscaling Methods. For hydrological and agricultural analyses, HadCM3 and PCM output was statistically downscaled to a 1/8° grid (≈150 km^2) (6) and to individual weather stations (7) for analyses of temperature and precipitation extremes and health impacts. Downscaling to the 1/8° grid used an empirical statistical technique that maps the probability density functions for modelled monthly precipitation and temperature for the climatological period (1961–1990) onto those of gridded historical observed data, so the mean and variability of observations are reproduced by the climate model data. The bias correction and spatial disaggregation technique is one originally developed for adjusting General Circulation Model output for long-range streamflow forecasting (6), later adapted for use in studies examining the hydrologic impacts of climate change (8), and compares favorably to different statistical and dynamic downscaling techniques (9) in the context of hydrologic impact studies.

Station-level downscaling for analyses of temperature and precipitation extremes and health impacts used a deterministic method in which grid-cell values of temperatures and precipi-

Freely available online through the PNAS open access option.

Abbreviations: DJF, December, January, February; HadCM3, Hadley Centre Climate Model, version 3; JJA, June, July, August; PCM, Parallel Climate Model; SRES, Special Report on Emission Scenarios; SWE, snow water equivalent.

[b]To whom correspondence should be addressed. E-mail: hayhoe@atmosresearch.com.

Table 1. Summary of midcentury (2020–2049) and end-of-century (2070–2099) climate and impact projections for the HadCM3 and PCM B1 and A1fi scenarios

			2020–2049				2070–2099			
			PCM		HadCM3		PCM		HadCM3	
	Units	1961–1990	B1	A1fi	B1	A1fi	B1	A1fi	B1	A1fi
Change in statewide avg temperatures										
Annual	°C	15.0	1.35	1.5	1.6	2.0	2.3	3.8	3.3	5.8
Summer (JJA)	°C	22.8	1.2	1.4	2.2	3.1	2.15	4.1	4.6	8.3
Winter (DJF)	°C	7.6	1.3	1.2	1.4	1.45	2.15	3.0	2.3	4.0
Change in statewide avg precipitation										
Annual	mm	544	−37	−51	+6	−70	+38	−91	−117	−157
Summer (JJA)	mm	20	−3	+2	−1	−7	+4	−46	−5	−1
Winter (DJF)	mm	269	−45	−55	+4	−44	+13	−13	−79	−92
Sea level rise	cm	—	8.7	9.5	11.6	12.7	19.2	28.8	26.8	40.9
Heatwave days										
Los Angeles	Days	12	28	35	24	36	44	76	47	95
Sacramento	Days	58	91	101	93	104	109	134	115	138
Fresno	Days	92	113	120	111	116	126	147	126	149
El Centro	Days	162	185	185	176	180	191	213	197	218
Length of heatwave season*	Days	115	135	142	132	141	149	178	162	204
Excess mortality for Los Angeles†										
Without acclimatization	avg no. of deaths/yr	—	—	—	—	—	394	948	667	1,429
With acclimatization	avg no. of deaths/yr	165	—	—	—	—	319	790	551	1,182
Change in April 1 snowpack SWE										
1,000–2,000 m elevation	%	3.6 km³	−60	−56	−58	−66	−65	−95	−87	−97
2,000–3,000 m elevation	%	6.5 km³	−34	−34	−24	−36	−22	−73	−75	−93
3,000–4,000 m elevation	%	2.3 km³	−11	−15	4	−16	15	−33	−48	−68
All elevations	%	12.4 km³	−38	−37	−26	−40	−29	−73	−72	−89
Change in annual reservoir inflow‡										
Total	%	21.7 km³	−18	−22	5	−10	12	−29	−24	−30
Northern Sierra	%	15.2 km³	−19	−22	3	−9	9	−29	−20	−24
Southern Sierra	%	6.5 km³	−16	−23	10	−14	17	−30	−33	−43
Change in April–June reservoir inflow‡										
Total	%	9.1 km³	−20	−24	−11	−19	−1	−46	−41	−54
Northern Sierra	%	5.5 km³	−21	−24	−16	−19	−6	−45	−34	−47
Southern Sierra	%	3.6 km³	−18	−24	−2	−19	5	−47	−52	−65
Change water year flow centroid‡										
Total	Days	03/26	0	2	−15	−7	−7	−14	−23	−32
Northern Sierra	Days	03/13	0	3	−16	−5	−3	−11	−18	−24
Southern Sierra	Days	05/01	−10	−7	−19	−12	−22	−34	−34	−43

avg, average; JJA, June, July, August; DJF, December, January, February; SWE, snow water equivalent.

*The number of days between the beginning of the year's first and end of the year's last heatwave.

†Reference period is 1990–1999, and projections are for the period 2090–2099.

‡Results are for inflows to seven major dams and reservoirs in the Sacramento/San Joaquin water system, including three in the Northern Sierra (Shasta, Oroville, and Folsom) and four in the Southern Sierra (New Melones, New Don Pedro, Lake McClure, and Pine Flat).

tation from the reference period were rescaled by simple monthly regression relations to ensure that the overall probability distributions of the simulated daily values closely approximated the observed probability distributions at selected long-term weather stations (7). The same regression relations were then applied to future simulations, such that rescaled values share the weather statistics observed at the selected stations. At the daily scales addressed by this method, the need to extrapolate beyond the range of the historically observed parts of the probability distributions was rare even in the future simulations (typically $<1\%$ of the future days) because most of the climate changes involve more frequent warm days than actual truly warmer-than-ever-observed days (7).

Except where otherwise noted, we present projected climate anomalies and impacts averaged over 2020–2049 (with a midpoint of 2035) and 2070–2099 (here designated as end-of-century, with a midpoint of 2085), relative to a 1961–1990 reference period.

Temperature. All simulations show increases in annual average temperature before midcentury that are slightly greater under the higher A1fi emissions scenario (see Fig. 4, which is published as supporting information on the PNAS web site). By end-of-century, projected temperature increases under A1fi are nearly twice those under B1, with the more sensitive HadCM3 model producing larger absolute changes (Table 1). Downscaled seasonal mean temperature projections (10) show consistent spatial patterns across California, with lesser warming along the southwest coast and increasing warming to the north and northeast (Fig. 1). Statewide, the range in projected average temperature increases is higher than previously reported (11–14), particularly for summer temperature increases that are equal to or greater than increases in winter temperatures.

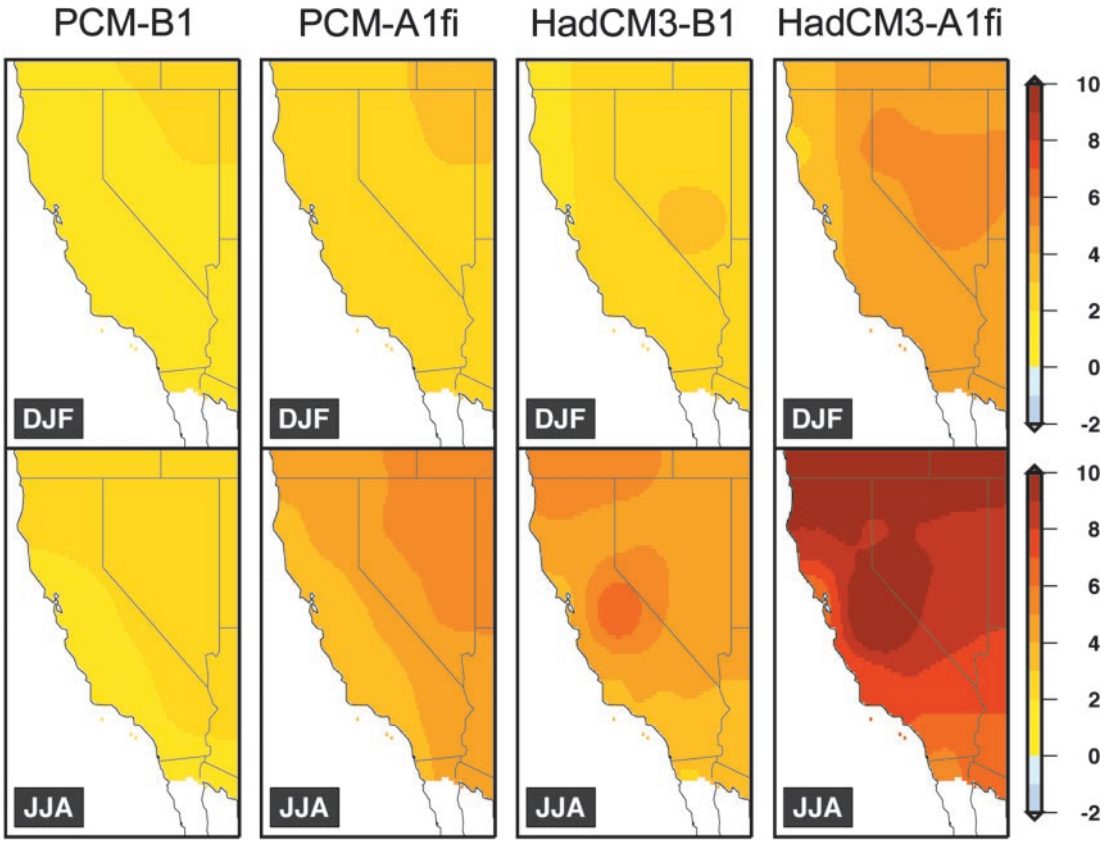

Fig. 1. Downscaled winter (DJF) and summer (JJA) temperature change (°C) for 2070–2099, relative to 1961–1990 for a 1/8° grid. Statewide, SRES B1 to A1fi winter temperature projections for the end of the century are 2.2–3°C and 2.3–4°C for PCM and HadCM3, respectively, compared with previous projections of 1.2–2.5°C and 3–3.5°C for PCM and HadCM2, respectively. End-of-century B1 to A1fi summer temperature projections are 2.2–4°C and 4.6–8.3°C for PCM and HadCM3, respectively, compared with previous projections of 1.3–3°C and 3–4°C for PCM and HadCM2, respectively (11–14).

Precipitation. Precipitation shows a tendency toward slight decreases in the second half of the century with no obvious interscenario differences in magnitude or frequency (see Figs. 5–10, which are published as supporting information on the PNAS web site). Three of four simulations project winter decreases of −15% to −30%, with reductions concentrated in the Central Valley and along the north Pacific Coast. Only PCM B1 projects slight increases (≈7%) by the end of the century (Table 1). These results differ from previous projections showing precipitation increases of 75–200% by 2100 (11–13), but they are consistent with recent PCM-based midrange projections (14, 15). The larger-scale pattern of rainfall over North America is more uniform across scenarios, showing an area of decreased (or lesser increase in) precipitation over California that contrasts with increases further up the coast (see Fig. 11, which is published as supporting information on the PNAS web site). Because interdecadal variability often dominates precipitation over California, projected changes in climate and impacts associated with the direct effects of temperature should be considered more robust than those determined by interactions between temperature and precipitation or precipitation alone.

Extreme Heat and Heat-Related Mortality

Temperature extremes increase in both frequency and magnitude under all simulations, with the most dramatic increases occurring under the A1fi scenario. Changes in local temperature extremes were evaluated based on exceedance probability analyses, by using the distribution of daily maximum temperatures downscaled to representative locations (16). Exceedance probabilities define a given temperature for which the probability exists that X% of days throughout the year will fall below that temperature (i.e., if the 35°C exceedance probability averages 95% for the period 2070–2099, this means that an average of 95% or ≈347 days per year are likely to lie below 35°C). For the four locations examined for extreme heat occurrence (Los Angeles, Sacramento, Fresno, and Shasta Dam), mean and maximum temperatures occurring 50% and 5% of the year increase by 1.5–5°C under B1 and 3.5–9°C under A1fi by the end of the century. Extreme temperatures experienced an average of 5% of the year during the historical period are also projected to increase in frequency, accounting for 12–19% (B1) and 20–30% (A1fi) of days annually by 2070–2099 (see Fig. 12, which is published as supporting information on the PNAS web site).

The annual number of days classified as heatwave conditions (3 or more consecutive days with temperature above 32°C) increases under all simulations, with more heatwave days under A1fi before midcentury (see Fig. 13, which is published as supporting information on the PNAS web site). Among the four locations analyzed, increases and interscenario differences are proportionally greatest for Los Angeles, a location that currently experiences relatively few heatwaves. By the end of the century, the number of heatwave days in Los Angeles increases four times under B1, and six to eight times under A1fi. Statewide, the length of the heatwave season increases by 5–7 weeks under B1 and by 9–13 weeks under A1fi by the end of this century, with interscenario differences emerging by midcentury (Table 1; see also Fig. 14, which is published information on the PNAS web site).

The connection between extreme heat and summer excess mortality is well established (17). Heat-related mortality estimates for the Los Angeles metropolitan area were determined

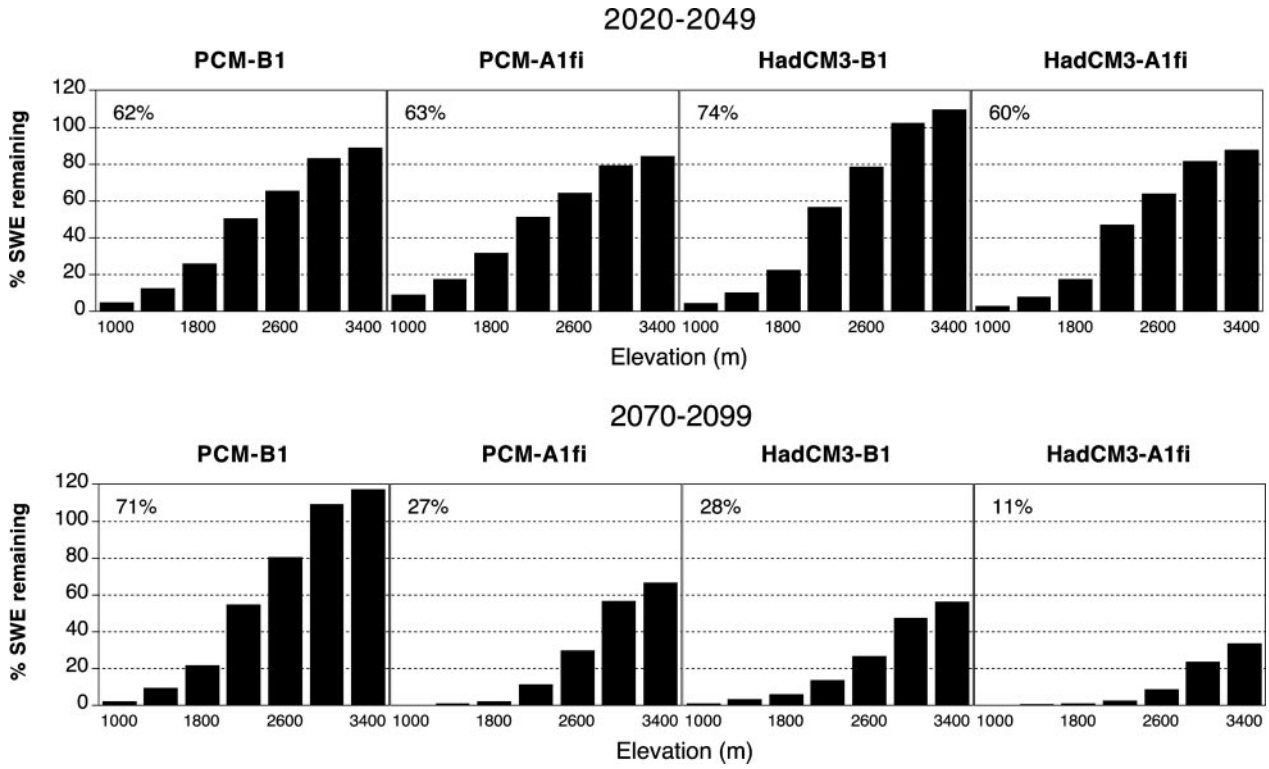

Fig. 2. Average snowpack SWE for 2020–2049 and 2070–2099 expressed as a percent of the average for the reference period 1961–1990 for the Sierra Nevada region draining into the Sacramento–San Joaquin river system. Total SWE losses by the end of the century range from 29–72% for the B1 scenario to 73–89% for the A1fi scenario. Losses are greatest at elevations below 3,000 m, ranging from 37–79% for B1 to 81–94% for A1fi by the end of the century. Increases in high elevation SWE for midcentury HadCM3 B1 and end-of-century PCM B1 runs result from increased winter precipitation in these simulations.

by threshold meteorological conditions beyond which mortality tends to increase. An algorithm was developed to determine the primary environmental factors (including maximum apparent temperature, number of consecutive days above the threshold apparent temperature, and time of year) that explain variability in excess mortality for all days with apparent maximum temperatures at or above the derived daily threshold apparent temperature (18) value of 34°C (see *Heat-Related Mortality* in *Supporting Text*). Estimates do not account for changes in population or demographic structure.

From a baseline of ≈165 excess deaths during the 1990s, heat-related mortality in Los Angeles is projected to increase by about two to three times under B1 and five to seven times under A1fi by the 2090s if acclimatization is taken into account (see *Heat-Related Mortality* in *Supporting Text*). Without acclimatization, these estimates are about 20–25% higher (Table 1). Actual impacts may be greater or lesser depending in part on demographic changes and societal decisions affecting preparedness, health care, and urban design. Individuals likely to be most affected include elderly, children, the economically disadvantaged, and those who are already ill (19, 20).

Impacts on Snowpack, Runoff, and Water Supply

Rising temperatures, exacerbated in some simulations by decreasing winter precipitation, produce substantial reductions in snowpack in the Sierra Nevada Mountains, with cascading impacts on California winter recreation, streamflow, and water storage and supply. Snowpack SWE was estimated by using daily, bias-corrected and spatially downscaled temperature and precipitation to drive the Variable Infiltration Capacity distributed land surface hydrology model. The Variable Infiltration Capacity model, using the resolution and parameterization also implemented in this study, has been shown to reproduce observed streamflows when driven by observed meteorology (10) and has been applied to simulate climate change (8) in this region. April 1 SWE decreases substantially in all simulations before midcentury (see Fig. 15, which is published as supporting information on the PNAS web site). Reductions are most pronounced at elevations below 3,000 m, where 80% of snowpack storage currently occurs (Table 1 and Fig. 2). Interscenario differences emerge before midcentury for HadCM3 and by the end of the century for both models. These changes will delay the onset of and shorten the ski season in California (see *Impact of Decreasing Snowpack on California's Ski Industry* in *Supporting Text*).

Water stored in snowpack is a major natural reservoir for California. Differences in SWE between the B1 and A1fi scenarios represent ≈1.7 km^3 of water storage by midcentury and 2.1 km^3 by the end of the century for HadCM3. For PCM, overall SWE losses are smaller, but the difference between the A1fi and B1 scenarios is larger by the end of the century, representing >4 km^3 of storage. Reductions for all simulations except PCM under the lower B1 emission scenario are greater than previous projections of diminishing snowpack for the end of the century (8, 21). By 2020–2049 the SWE loss is comparable to that previously projected for 2060 (22).

Warmer temperatures and more precipitation falling as rain instead of snow also causes snowmelt runoff to shift earlier under all simulations (Table 1), which is consistent with earlier studies (23). The magnitude of the shift is greater in the higher-elevation Southern basins and under the higher A1fi scenario. Stream inflows to major reservoirs decline because of diminished snowpack and increased evaporation before midcentury, except where winter precipitation increases (Table 1). The greater reductions in inflows seen under A1fi are driven by both higher temperatures and lower average precipitation as compared with B1.

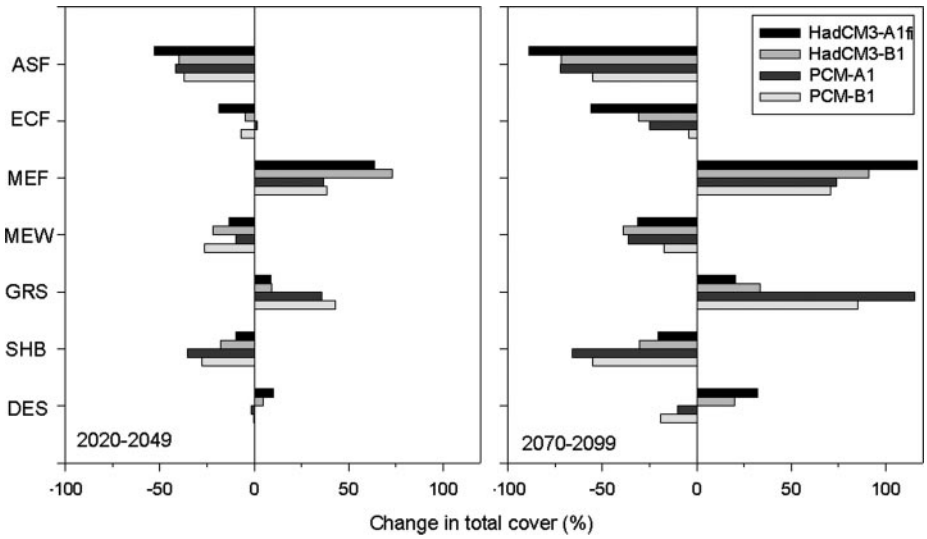

Fig. 3. Statewide change in cover of major vegetation types for 2020–2049 and 2070–2099, relative to simulated distributions for the 1961–1990 reference period. ASF, alpine/subalpine forest; ECF, evergreen conifer forest; MEF, mixed evergreen forest; MEW, mixed evergreen woodland; GRS, grassland; SHB, shrubland; DES, desert. Increasing temperatures drive the reduction in alpine/subalpine forest cover and cause mixed conifer forest to displace evergreen conifer forest in the Sierra Nevada Mountains and the North Coast. Mixed conifer forest in the South Coast expands because of increased humidity and reduced fire frequency. Because of drier conditions and increased fire frequency in inland locations, grassland displaces shrubland and woodland, particularly in the PCM simulations, whereas warmer and drier conditions under HadCM3 cause an expansion of desert cover in the southern Central Valley.

Earlier runoff may also increase the risk of winter flooding (7). Currently, state operators maintain ≈12 km^3 of total vacant space in the major reservoirs to provide winter and early spring flood protection,[n] a volume approximately equal to that stored in the natural snowpack reservoir by April 1st. Capturing earlier runoff to compensate for future reductions in snowpack would take up most of the flood protection space, forcing a choice between winter flood prevention and maintaining water storage for the summer and fall dry period use. Flood risk and freshwater supply are also affected by higher sea levels, which are projected to rise 10–40 cm under B1 and 20–65 cm under A1fi by 2100 (Table 1; see also Fig. 16, which is published as supporting information on the PNAS web site).

Declining Sierra Nevada snowpack, earlier runoff, and reduced spring and summer streamflows will likely affect surface water supplies and shift reliance to groundwater resources, already overdrafted in many agricultural areas in California (24). This could impact 85% of California's population who are agricultural and urban users in the Central Valley, San Francisco Bay Area, and the South Coast, about half of whose water is supplied by rivers of the Central Valley. Under A1fi (both models) and B1 (HadCM3), the projected length, frequency, and severity of extreme droughts in the Sacramento River system during 2070–2099 substantially exceeds what has been experienced in the 20th century. The proportion of years projected to be dry or critical increases from 32% in the historical period to 50–64% by the end of the century under all but the wetter PCM B1 scenario (see Table 2, which is published as supporting information on the PNAS web site). Changes in water availability and timing could disrupt the existing pattern of seniority in month-dependent water rights by reducing the value of rights to mid- and late-season natural streamflow and boosting the value of rights to stored water. The overall magnitude of impacts on water users depends on complex interactions between temperature-driven snowpack decreases and runoff timing, precipitation, future population increases, and human decisions regarding water storage and allocation (see *Impacts on Water Supply* in *Supporting Text*).

Impacts on Agriculture and Vegetation Distribution

In addition to reductions in water supply, climate change could impact California agriculture by increasing demand for irrigation to meet higher evaporative demand, increasing the incidence of pests (25), and through direct temperature effects on production quality and quantity. Dairy products (milk and cream, valued at $3.8 billion annually) and grapes ($3.2 billion annually) are the two highest-value agricultural commodities of California's $30 billion agriculture sector (26). Threshold temperature impacts on dairy production and wine grape quality were calculated by using downscaled temperature projections for key counties, relative to average observed monthly temperatures.[o]

For dairy production, losses were estimated for temperatures above a 32°C threshold (27), as well as for additional losses between 25°C (28) and 32°C. For the top 10 dairy counties in the state (which account for 90% of California's milk production), rising temperatures were found to reduce production by as much as 7–10% (B1) and 11–22% (A1fi) by the end of the century (see Table 3, which is published as supporting information on the PNAS web site). Potential adaptations may become less practical with increasing temperature and humidity (29).

For wine grapes, excessively high temperatures during ripening can adversely affect quality, a major determinant of market value. Assuming ripening occurs at between 1,150 and 1,300 biologically active growing degree days (30), ripening month was determined by summing modeled growing degree days above 10°C from April to October, for both baseline and projected scenarios. Monthly average temperature at the time of ripening was used to estimate potential temperature impacts on quality. For all simulations, average ripening occurs 1–2 months earlier and at higher temperatures, leading to degraded quality and marginal/impaired conditions for all but the cool coastal region

[n]See the U.S. Army Corps of Engineers Flood Control Requirements for California Reservoirs, Sacramento District Water Control Data System, Sacramento, CA (www.spk-wc.usace.army.mil).

[o]See Western U.S. Climate Historical Summaries (Western Regional Climate Center) at www.wrcc.dri.edu/climsum.html.

under all scenarios by the end of the century (see Table 3, which is published as supporting information on the PNAS web site). As with other perennial crops, adaptation options to shift varieties or locations of production would require significant time and capital investment.

The distribution of California's diverse vegetation types also changes substantially over the century relative to historical simulations (Fig. 3; see also Fig. 17, which is published as supporting information on the PNAS web site). Projections of changes in vegetation distribution are those given by MC1, a dynamic general vegetation model that simulates climate-driven changes in life-form mixtures and vegetation types; ecosystem fluxes of carbon, nitrogen, and water; and fire disturbance over time (31). Vegetation shifts driven primarily by temperature, such as reductions in the extent of alpine/subalpine forest and the displacement of evergreen conifer forest by mixed evergreen forest, are consistent across models and more pronounced under A1fi by the end of the century. Changes driven by precipitation and changes in fire frequency are model-dependent and do not exhibit consistent interscenario differences. Most changes are apparent before mid-century, with the exception of changes in desert cover. The shift from evergreen conifer to mixed evergreen forest and expansion of grassland are consistent with previous impact analyses (13), whereas the extreme reduction in alpine/subalpine forest and expansion of desert had not been reported in previous impacts assessments (12, 13).

Conclusions

Consistent and large increases in temperature and extreme heat drive significant impacts on temperature-sensitive sectors in California under both lower and higher emissions scenarios, with the most severe impacts occurring under the higher A1fi scenario. Adaptation options are limited for impacts not easily controlled by human intervention, such as the overall decline in snowpack and loss of alpine and subalpine forests. Although interscenario differences in climate impacts and costs of adaptation emerge mainly in the second half of the century, they are largely entrained by emissions from preceding decades (32). SRES scenarios do not explicitly assume climate-specific policy intervention, and thus this study does not directly address the contrast in impacts due to climate change mitigation policies. However, these findings support the conclusion that climate change and many of its impacts scale with the quantity and timing of greenhouse gas emissions (33). As such, they represent a solid starting point for assessing the outcome of changes in greenhouse gas emission trajectories driven by climate-specific policies (32, 34), and the extent to which lower emissions can reduce the likelihood and thus risks of "dangerous anthropogenic interference with the climate system" (35).

We thank Michael Dettinger and Mary Meyer Tyree for providing assistance with data and analysis, and Frank Davis for providing review of earlier drafts of this manuscript. PCM model results were provided by PCM personnel at the National Center for Atmospheric Research, and HadCM3 model results were provided by Dr. David Viner from the U.K. Met Office's Climate Impacts LINK Project. This work was supported in part by grants from the David and Lucile Packard Foundation, the William and Flora Hewlett Foundation, the Energy Foundation, the California Energy Commission, the National Oceanic and Atmospheric Administration Office of Global Programs, and the Department of Energy.

1. Nakićenović, N., Alcamo, J., Davis, G., de Vries, B., Fenhann, J., Gaffin, S., Gregory, K., Grübler, A., Jung, T. Y., Kram, T., *et al.* (2000) *Intergovernmental Panel on Climate Change Special Report on Emissions Scenarios* (Cambridge Univ. Press, Cambridge, U.K.).
2. Parry, M. (2002) *Global Environ. Change* **12** (3)**,** 149–153.
3. Washington, W. M., Weatherly, J. W., Meehl, G. A., Semtner, A. J., Bettge, T. W., Craig, A. P., Strand, W. G., Arblaster, J., Wayland, V. B., James, R. & Zhang, Y. (2000) *Clim. Dyn.* **16,** 755–774.
4. Gordon, C., Cooper, C., Senior, C. A., Banks, H., Gregory, J. M., Johns, T. C., Mitchell, J. F. B. & Wood, R. A. (2000) *Clim. Dyn.* **16,** 147–168.
5. Pope, V. D., Gallani, M. L., Rowntree, P. R. & Stratton, R. A. (2000) *Clim. Dyn.* **16,** 123–146.
6. Wood, A. W., Maurer, E. P., Kumar, A. & Lettenmaier, D. P. (2002) *J. Geophys. Res.* **107,** 4429, 10.1029/2001JD000659.
7. Dettinger, M. D., Cayan, D. R., Meyer, M. K. & Jeton, A. E. (2004) *Clim. Change* **62,** 283–317.
8. VanRheenan, N. T., Wood, A. W., Palmer, R. N. & Lettenmaier, D. P. (2004) *Clim. Change* **62,** 257–281.
9. Wood, A. W., Leung, L. R., Sridhar, V. & Lettenmaier, D. P. (2004) *Clim. Change* **62,** 189–216.
10. Maurer, E. P., Wood, A. W., Adam, J. C., Lettenmaier, D. P. & Nijssen, B. (2002) *J. Clim.* **15,** 3237–3251.
11. Field, C. B., Daily, G. C., Davis, F. W., Gaines, S., Matson, P. A., Melack, J. & Miller, N. L. (1999) *Confronting Climate Change in California: Ecological Impacts on the Golden State* (Union of Concerned Scientists, Cambridge, MA, and Ecological Society of America, Washington, DC).
12. Wilkinson, R., Clarke, K., Goodchild, M., Reichman, J. & Dozier, J. (2002) *The Potential Consequences of Climate Variability and Change for California: The California Regional Assessment* (U.S. Global Change Research Program, Washington, DC).
13. Wilson, T., Williams, L., Smith, J. & Medelsohn, R. (2003) *Global Climate Change and California: Potential Implications for Ecosystems, Health, and the Economy*, Publication No. 500-03-058CF (California Energy Commission, Public Interest Energy Research Environmental Area, Sacramento).
14. Leung, L. R., Qian, Y., Bian, X., Washington, W. M., Han, J. & Roads, J. O. (2004) *Clim. Change* **62,** 75–113.
15. Snyder, M. A., Bell, J. L., Sloan, L. C., Duffy, P. B. & Govindasamy, B. (2002) *Geophys. Res. Lett.* **29,** 1514–1517.
16. Miller, N. L., Bashford, K. E. & Strem, E. (2003) *J. Am. Water Resour. Assoc.* **39,** 771–784.
17. Kalkstein, L. S. & Davis, R. E. (1989) *Ann. Assoc. Am. Geogr.* **79,** 44–64.
18. Watts, J. D. & Kalkstein, L. S. (2004) *J. Appl. Meteorol.* **43,** 503–513.
19. McGeehin, M. A. & Mirabelli, M. (2001) *Environ. Health Perspect.* **109,** 185–189.
20. Chestnut, L. G., Breffle, W. S., Smith, J. B. & Kalkstein, L. S. (1998) *Environ. Sci. Policy* **1,** 59–70.
21. Knowles, N. & Cayan, D. R. (2002) *Geophys. Res. Lett.* **29,** 1891–1895.
22. Knowles, N. & Cayan, D. R. (2004) *Clim. Change* **62,** 319–336.
23. Gleick, P. H. & Chalecki, E. L. (1999) *J. Am. Water Resour. Assoc.* **35,** 1429–1441.
24. California Department of Water Resources, Division of Planning and Local Assistance (1998) *Bulletin 160–98: California Water Plan* (California Department of Water Resources, Sacramento).
25. Harrington, R. & Stork, N. E., eds. (1995) *Insects in a Changing Environment* (Academic, London).
26. California Agricultural Statistics Service (2002) *California Agriculture Statistical Review* (California Agricultural Statistics Service, Sacramento).
27. Ahmed, M. M. M. & El Amin, A. I. (1997) *J. Arid Environ.* **35,** 737–745.
28. Mellado, M. (1995) *Veterinaria* **26,** 389–399.
29. Pittock, B., Wratt, D., Basher, R., Bates, B., Finlayson, M., Gitay, H., Woodward, A., Arthington, A., Beets, P., Biggs, B., *et al.* (2001) in *Climate Change 2001: Impacts, Adaptation, and Vulnerability* (Cambridge Univ. Press, Cambridge, U.K.).
30. Gladstones, J. (1992) *Viticulture and Environment* (Winetitles, Underdale, South Australia), 310 pp.
31. Lenihan, J., Drapek, R., Bachelet, D. & Neilson, R. (2003) *Ecol. Appl.* **13,** 1667–1681.
32. Swart, R., Mitchell, J., Morita, T. & Raper, S. (2002) *Global Environ. Change* **12,** 155–165.
33. Houghton, J. T., Ding, Y., Griggs, D. J., Noguer, M., van der Linden, P. J. & Xiaosu, D., eds. (2001) *Climate Change 2001: The Scientific Basis* (Cambridge Univ. Press, Cambridge, U.K.).
34. Arnell, N. W., Livermore, M. J. L., Kovats, S., Levy, P. E., Nicholls, R., Parry, M. L. & Gaffin, S. R. (2004) *Global Environ. Change* **14,** 3–20.
35. United Nations (1992) *United Nations Framework Convention on Climate Change* (United Nations, Rio de Janeiro, Brazil).